https://doi.org/10.5194/egusphere-2025-496
Preprint. Discussion started: 6 March 2025

2D Seismic Imaging of the Koillismaa Layered Igneous Complex, North-Eastern Finland

Brij Singh[1], Andrzej Górszczyk[1], Michał Malinowski[1,2], Suvi Heinonen[3], Uula Autio[2], Tuomo Karinen[2], Marek Wojdyła[4], and the SEEMS DEEP Working Group*

[1]Institute of Geophysics, Polish Academy of Sciences Warsaw, Księcia Janusza 64, 01-452 Warsaw, Poland
[2]Geological Survey of Finland, Vuorimiehentie 5, 02151 Espoo, Finland
[3]Institute of Seismology, University of Helsinki, PO BOX 68 (Pietari Kalmin katu 5), Helsinki, Finland
[4]Geopartner Geofizyka Sp. z o.o., Skośna 39B, 30-383, Kraków, Poland
*A full list of authors appears at the end of the paper

Correspondence to: Brij Singh (bsingh@igf.edu.pl)

Abstract. The Seismic and Electromagnetics Methods for Deep mineral exploration (SEEMS DEEP) project is associated with the Koillismaa Layered Igneous Complex (KLIC) in north-eastern Finland. The KLIC is characterized by a Bouguer positive gravity and magnetic anomaly zone connecting the two exposed ends of the KLIC i.e. the Koillismaa intrusion and the Näränkävaara intrusion. The KLIC has the potential to host several critical raw minerals, like nickel and cobalt which are included in the European Union's critical raw material list. For this purpose, two regional seismic profiles were acquired to map the regional reflectivity in the area, constraining the large-scale information about the geological architecture of KLIC. Seismic imaging delineated reflectivity up to a depth of ~5 – 6 km with several reflective packages at various depths which may be representative of the presence of dykes, faults, and major lithological contacts present in the area. Several regional faults were also imaged. The top of the magma conduit associated with KLIC was successfully mapped with hints of fault-like events cross-cutting the intrusion revealing a more complex internal structure that was earlier assumed of as a single lithological unit. It was interpreted that a second magma conduit might exist between the Koillismaa intrusion and the Näränkävaara Intrusion. Results were compared against the available petrophysical data and a preliminary available geological model based on the density model of the gravity inversion with constraints from the drillhole data.

Keywords

Land seismics; curvelet; regional reflectivity; Koillismaa; Layered igneous intrusion; Näränkävaara intrusion

1. Introduction

The demand for raw materials has increased rapidly in recent times for various reasons: high-tech solutions, developing green energy, pushing towards a carbon-neutral society, sustainability, etc. (European Commission Report, 2023). Therefore, it is required to explore newer and deeper targets to sustain the supply and demand equilibrium. Ore deposits associated with mafic to ultramafic igneous rocks hold great potential to fulfil this requirement (Ripley and Li, 2018). The Koillismaa Layered Intrusion Complex has been of interest among geologists for several decades due to its potential to host critical raw materials

https://doi.org/10.5194/egusphere-2025-496
Preprint. Discussion started: 6 March 2025

(Alapieti, 1982; Karinen, 2010). The rocks of similar lithologies worldwide were found to be rich in Ni-Cu-Co-PGE and Cr-V-Ti-Fe type deposits (Barnes et al., 2016; Schulz et al., 2014). Many of these minerals like nickel, copper, cobalt, lithium, titanium metal, vanadium, etc., are in the European Union's strategic raw material list (EU Critical Raw Materials Act, 2024).

The KLIC is composed of two exposed mafic-ultramafic layered intrusions i.e. Koillismaa intrusion in the west and Näränkävaara intrusion in the east (Fig. 1). These intrusions are linked by a high gravity and magnetic anomaly zone: the Koillismaa Deep Anomaly (KDA) which has been recognized since the earliest ground gravimetric and airborne geophysical measurements conducted in the 1950s (Karinen, 2010; Salmirinne and Iljina, 2003). In 2018, the Geological Survey of Finland (GTK) acquired a low-fold 2D seismic profile in the Koillismaa area delineating a weak reflectivity at ~1.3 km and a stronger reflectivity at ~3.3 km depth which was tentatively interpreted as the top and bottom of the intrusion (KOSE2018 profile, Gislason et al., 2019). In 2020, GTK's Koillismaa deep drillhole project confirmed the presence of mafic-ultramafic plutonic rocks at a depth of ~1.4 km. Petrophysical and lab studies were done on the collected core samples from the drillhole, supplemented by limited wireline-logging data (Heinonen et al., 2022; Nousiainen et al., 2022). A deep-seated magma conduit system, named Koillismaa Feeder connects the exposed intrusion of the complex i.e. Koillismaa Intrusion and Näränkävaara Intrusion was inferred (Karinen et al., 2021b; Tirronniemi et al., 2024). This makes KLIC an interesting area to be studied in greater detail.

Geophysical surveys for mineral exploration have been routinely accomplished by potential field methods, electromagnetics, electrical methods, etc., but they lack higher resolution at deeper depths required to distinguish different lithologies. In comparison, seismic reflection surveys can provide higher-resolution images of the subsurface and have now emerged as an established method for deep mineral exploration in the hardrock environment (also called crystalline environment) (Malehmir et al., 2012). Three-dimensional (3D) surveys are often conducted for detailed mapping of the mineralization, whereas two-dimensional (2D) surveys are an excellent choice for affordable regional assessment (Bellefleur et al., 2015; Cheraghi et al., 2020; Milkereit et al., 2000; Nedimović and West, 2003 and references therein). 2D surveys also serve as a good instrument for the initial seismic assessment of the area and can form a basis for the development of a full-scale 3D survey. It is cheaper, faster, and logistically simpler than 3D surveys (Malehmir et al., 2017; Markovic et al., 2020), but one has to be careful when interpreting 2D profiles crossing complex 3D geology.

With this aim, the Seismic and Electromagnetics Methods for Deep mineral exploration (SEEMS DEEP) project (2022–2025) was funded under the ERA-MIN 3 consortium to study the underlying geological setting of KLIC in greater detail using an integrated approach of seismics and electromagnetic methods (Autio et al., 2024). Apart from being a method-development playground, the project aims to improve our understanding of the geology of the Koillismaa area. Two regional crooked 2D reflection seismic profiles were acquired along with a 3D seismic survey (see details in Malinowski et al., 2024) in August 2023 in the vicinity of the Koillismaa drillhole. In this article, we are focusing on the results obtained from the 2D seismic

https://doi.org/10.5194/egusphere-2025-496
Preprint. Discussion started: 6 March 2025

profiles. Our main objective is to map the regional reflectivity in the area, supported by the petrophysical data, and to constrain the first-order geometry of the unexposed part of KLIC.

2. Geology of the area, previous geophysical studies, and petrophysical analysis

The Fennoscandian Shield hosts numerous ~2.51–2.43 Ga mafic-ultramafic layered intrusions which were formed during the magmatism that led to the breakup of one or more Archaean cratons (Bleeker and Ernst, 2006; Ciborowski et al., 2015; Heaman, 1997; Köykkä et al., 2022; Skyttä et al., 2019). The Fennoscandian mafic-ultramafic intrusions are regarded as very prospective for hosting mineralization associated with critical raw materials. The ~2.44 Ga KLIC as part of the Fennoscandian Shield is a ~50 – 60 km long mafic-ultramafic layered intrusion in north-eastern Finland (Karinen, 2010). The two exposed intrusions of KLIC i.e. the Koillismaa Intrusion and the Näränkävaara Intrusion (Fig. 1), are linked by a ~50 km long positive gravity and magnetic anomaly (Karinen, 2010; Salmirinne and Iljina, 2003). Previous interpretations of the observed Bouguer anomaly suggested a mafic dyke-like intrusion (magma conduit) of about ~2.5 – 4 km in width, and the depth from the top at ~1 – 2 km (see Fig. 1a) (Salmirinne and Iljina, 2003).

GTK acquired a low-fold 2D seismic profile in the KDA area in 2018 as a part of the siting study before the deep research drilling project. The seismic survey profile named KOSE2018 (Fig. 2), delineated the top of the intrusion at ~1.3 km as a weak reflector and the bottom at ~3.3 km depth with stronger reflectivity (Gislason et al., 2019). In 2020–2021, a diamond drillhole next to the survey profile (red star in Fig. 1, drillhole shown in Fig. 2 and Fig. 3) confirming the presence of the ultramafic rocks at a depth of more than ~1.4 km (Karinen et al., 2021b; Tirronniemi et al., 2024), thus verifying the presence of a deep-seated magma conduit system connecting the exposed intrusions of the complex (Karinen et al., 2021a). Extensive petrophysical and lab studies were performed on the collected drill core samples and classifications were made of different lithologies and rock types (Heinonen et al., 2022; Nousiainen et al., 2022). As per these studies, the surface bedrock geology at the Koillismaa study site is mainly composed of homogenous orthogneisses, cross-cutting diabase dykes, and a narrow belt of banded iron formations. The magma conduit at the depth is characterized by the mafic-ultramafic rocks such as peridotites, pyroxenites, and gabbronorites.

A plot of P-wave velocity, density, reflection coefficient series, and the corresponding synthetic seismogram are shown in Figure 3(a-d). The synthetic seismogram is produced using the Ricker wavelet with a dominant frequency of 35 Hz. A simplified lithology of the borehole is shown in Figure 3e (red star in Fig. 1, and Fig. 2). Average seismic P-wave velocity ranges between ~5.5 – 6.5 km/s and density between ~2800 – 3200 kg/m^3 for mafic-ultramafic rocks (as measured on the core samples under the room temperature and pressure conditions). A clear acoustic impedance contrast was found between the ultramafics and the overlying felsic rocks with the presence of several cross-cutting diabase veins in the vicinity of the drill hole (see synthetic seismogram, Fig. 3d). These faults/fractures and lithology changes were also imaged during the walkaway

https://doi.org/10.5194/egusphere-2025-496
Preprint. Discussion started: 6 March 2025

vertical seismic profiling (VSP) survey conducted in the same drillhole (Malinowski et al., 2023; Tirronniemi et al., 2024). A preliminary geological model was created mainly based on the limited surface geological data, potential field inversions, and resistivity models from sparse MT stations with constraints from the existing drillhole data.

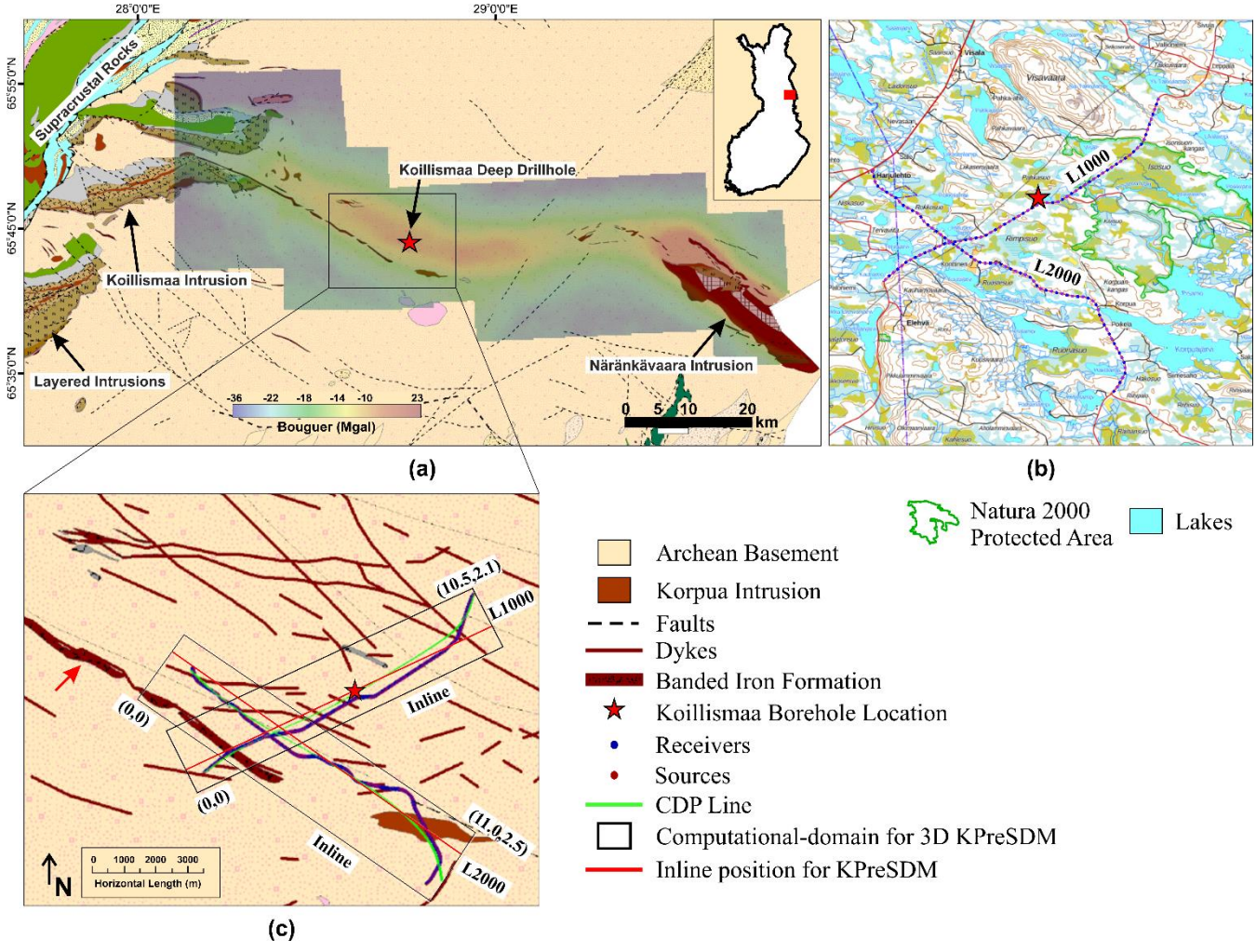

Figure 1: (a) Generalized geological map of the KLIC with Koillismaa intrusion in the west and Näränkävaara intrusion in the east. The location of the area is shown by the red rectangle over the map of Finland in the top-right inset (© Google Maps). A Bouguer gravity anomaly map is overlaid over the geological map. The red star marks the Koillismaa drillhole (b) Seismic profiles (L1000 and L2000) overlaid on the topographic map. (c) Acquisition profiles overlaid over the geological map. Purple and blue dots mark the position of the shotpoints and receivers respectively. The green lines show the processing lines (CDP binning line) for each profile. The black box shows the computational domain for depth migration (in km). The red line shows the position of the inline at which the results from Kirchhoff prestack depth migration (KPreSDM) are shown in Fig. 5b and 6b.

https://doi.org/10.5194/egusphere-2025-496
Preprint. Discussion started: 6 March 2025

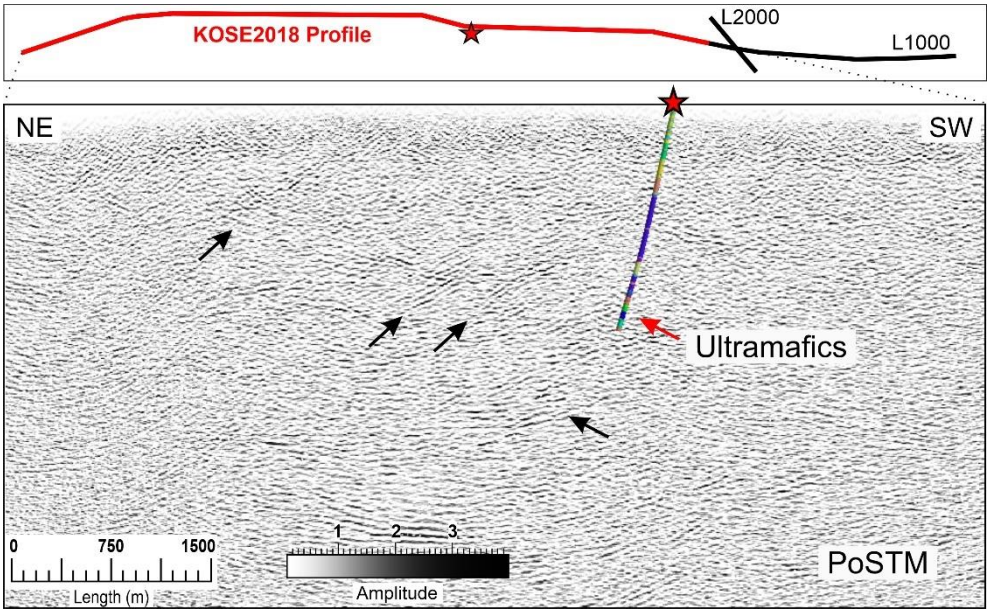

Figure 2: KOSE2018 2D seismic profile (Gislason et al., 2019). The top panel shows the map view of the overlapping KOSE2018 profile (red) with the SEEMS DEEP profile L1000 (in black). Black arrows in the bottom panel mark different reflectors mapped in the area (compare with Fig. 5a). The borehole is plotted for different lithologies based on the analysis of Koillismaa drill core data (red star, Fig. 1). A simplified lithology for the same is shown in Fig. 3e.

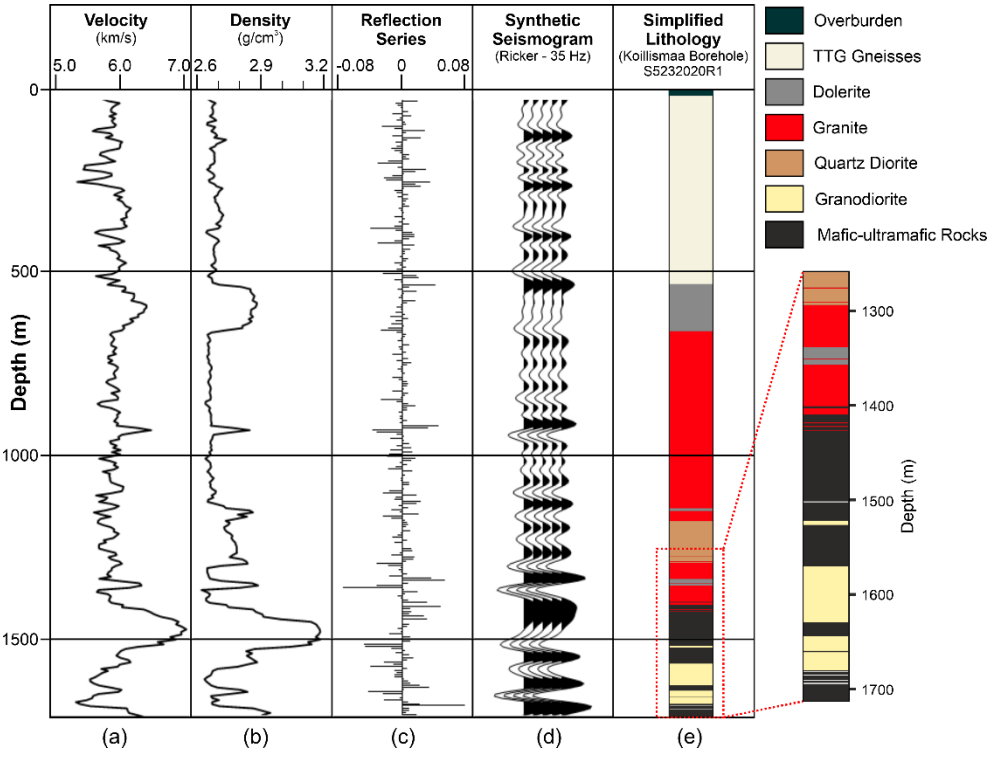

https://doi.org/10.5194/egusphere-2025-496
Preprint. Discussion started: 6 March 2025

Figure 3: (a), (b), and (c) Plot of P-wave velocity, density, and reflection coefficient series based on laboratory measurements on core samples from the Koillismaa drillhole (red star, Fig. 1), (d) Synthetic seismogram produced using a Ricker wavelet with dominant frequency 35 Hz highlighting the acoustic impedance contrast between different lithologies, (e) Simplified lithology of the drillhole (same as in Fig. 2). Drilling shows the surface bedrock geology to be composed of homogenous orthogneisses, cross-cutting dykes and the magma conduit characterized by the mafic-ultramafic rocks at an approx. depth of ~1.4 km.

3. Data Acquisition

The dataset comprises two crooked regional reflection seismic profiles. The first profile, L1000 is ~10.5 km long and is oriented in the NE-SW direction roughly intersecting the mafic intrusion perpendicular to its strike (see Fig. 1a and 1c). The second profile, L2000 is ~11.5 km long and is oriented in the NW-SE direction (Fig. 1c). Both profiles have a uniform receiver spacing of 15 m and shot spacing of 30 m. Blue dots mark receivers and purple dots mark shots overlapping the receiver points (Fig. 1c). Geospace's GS-ONE Low-Frequency three-component (3C) land geophones with a natural frequency of 5 Hz Hz were used with GSB3-3C recording units in a continuous mode for both profiles. A 22-tonne Mark IV Vibroseis truck was used as the source along the existing gravel roads (see map in Fig. 1b). All the acquisition parameters related to the survey are summarised in Table 1. The acquired data are of good quality with reflections visible in the raw shot gathers (Fig. 4, red arrows). The data is of better quality for shotpoints located in the southern and western end of the survey for which the first-break energy was visible for the full-offset range, otherwise, an effective offset of ~4 – 5 km is generally observed for the rest of the shots.

Table 1. Acquisition parameters for profiles L1000 and L2000

Data Acquisition	L1000	L2000
Spread Configuration	Fixed-spread geometry	
Receiver Spacing	15 m	
Receiver Type	3C geophone, 3C recording node	
Source Spacing	30 m	
Source Type	Vibroseis (22-ton Mark IV)	
Vibroseis Sweep	20 – 160 Hz +1dB (20-s sweep length)	
Record Length	6 s	
Number of Sweeps/Shot Point	3	
Profile Length	~10.5 km	~11.5 km
Channels	701	746
Vibroseis Source Points	348	371
Maximum CDP Fold	~417	~453
Elevation Changes	~246 – 268 m	~244 – 262 m

https://doi.org/10.5194/egusphere-2025-496
Preprint. Discussion started: 6 March 2025

4. Data Processing

Reflection seismic data processing for both profiles followed the standard processing workflow applied to the hardrock seismics. Data preprocessing started with the extraction of the vertical component from the 3C receiver data. A crooked-line geometry was set up with rectangular bin geometry. Common Depth Point (CDP) bin spacing was kept at half of the receiver spacing sufficient to map the steeply dipping diabase veins, fault, etc. present in the area. The CDP processing line for both profiles is shown by the green line in Figure 1c. Bad traces were removed and manual picking of first-break energy for the full offset range was done for both profiles (see Fig. 4a and 4d).

Preprocessing involved a two-layered refraction statics solution with a replacement velocity of 5 km/s to handle the heterogeneous near-surface weathering layer. A floating datum at elevation 300 m above sea level (a.s.l.) was defined to account for the differences in the elevation of the source and receivers. It was followed by spherical divergence correction, automatic gain control (AGC), and deconvolution. A combination of spiking deconvolution and gapped deconvolution was found most effective in enhancing the data reflectivity. A notch filter was applied to remove the mono-frequencies. An airwave mute, 1D median filter, and bandpass filter (BP) were used to attenuate the ground roll and surface waves (compare Figure 4a with 4b, and 4d with 4e). An offset-based refraction mute ~30 ms below the first break was used. A special emphasis at the pre-processing stage was placed on improving the coherency of the signal of the common shot gathers with curvelet denoising (Górszczyk et al., 2015) (compare Figure 4b with 4c, and 4e with 4f).

Velocities were picked on the prestack gathers resulting in the normal moveout (NMO) correction velocities in the range of ~5.7 – 6.2 km/s. However, due to the uniformity of P-wave velocity associated with homogenous geology above the target area i.e. mafic-ultramafic rocks (~1.4 km); a constant velocity of 6 km/s was found to produce similarly good results when used for the NMO followed by the dip moveout correction (DMO). Final migration tests were performed for a scan of velocities in the range of ~5.0 – 6.5 km to assess the overall imaging of different units.

A square-root normalization stacking was done on the DMO corrected shot gathers followed by FX-Deconvolution and BP filtering. Stolt (f-k) migration with a constant velocity of 6 km/s produced optimum results aiming at the target area. We also tested prestack time migration which produced better imaging in some areas but overall, DMO followed by PoSTM produced qualitatively better imaging results (with less migration artifacts). Finally, the processed time sections were converted into depth sections, and data was exported for visualization. All time-domain processing parameters are summarized in Table 2.

Table 2. Time-domain processing workflow for profiles L1000 and L2000

Data Preprocessing	
Data Extraction	vertical component
Data Read	SEG-Y, 3.0 s

https://doi.org/10.5194/egusphere-2025-496
Preprint. Discussion started: 6 March 2025

Geometry Setup	crooked line, rectangular bin
Nominal CDP Spacing	7.5 m
Trace Editing	bad traces removed
First-Break Picking	manual pick
Preprocessing Stage	
Refraction Statics	2-layer model, repl. vel. – 5 km/s
Floating Datum	300 m a.s.l.
Spherical Divergence Correction	v^2t function
AGC	250 m
Deconvolution	Spiking, 150 ms / Gapped, 150 / 24 ms
Notch Removal	50 / 100 Hz
Airwave Mute	330 m/s
Linear Noise Removal	Median filter, vel. – 2.8/3.0 km/s
Bandpass Filter (BP)	15-35-145-185 Hz
AGC	250 ms
Refraction Mute	offset-based, 30 ms below first-arrivals
Coherency Enhancement	Curvelet-denoising
NMO	const. velocity – 6 km/s
Dip Moveout	const. velocity – 6 km/s
Stacking and Migration	
Stacking	SQRT Normalization
FX-Deconvolution	11 traces (100 /30 ms window)
Final Datum	300 m a.s.l.
Migration	Stolt (6 km/s)
BP	15-35-145-185 Hz
Time-to-depth Conversion	Vel. – 6 km/s
Data Export	SEGY format

https://doi.org/10.5194/egusphere-2025-496
Preprint. Discussion started: 6 March 2025

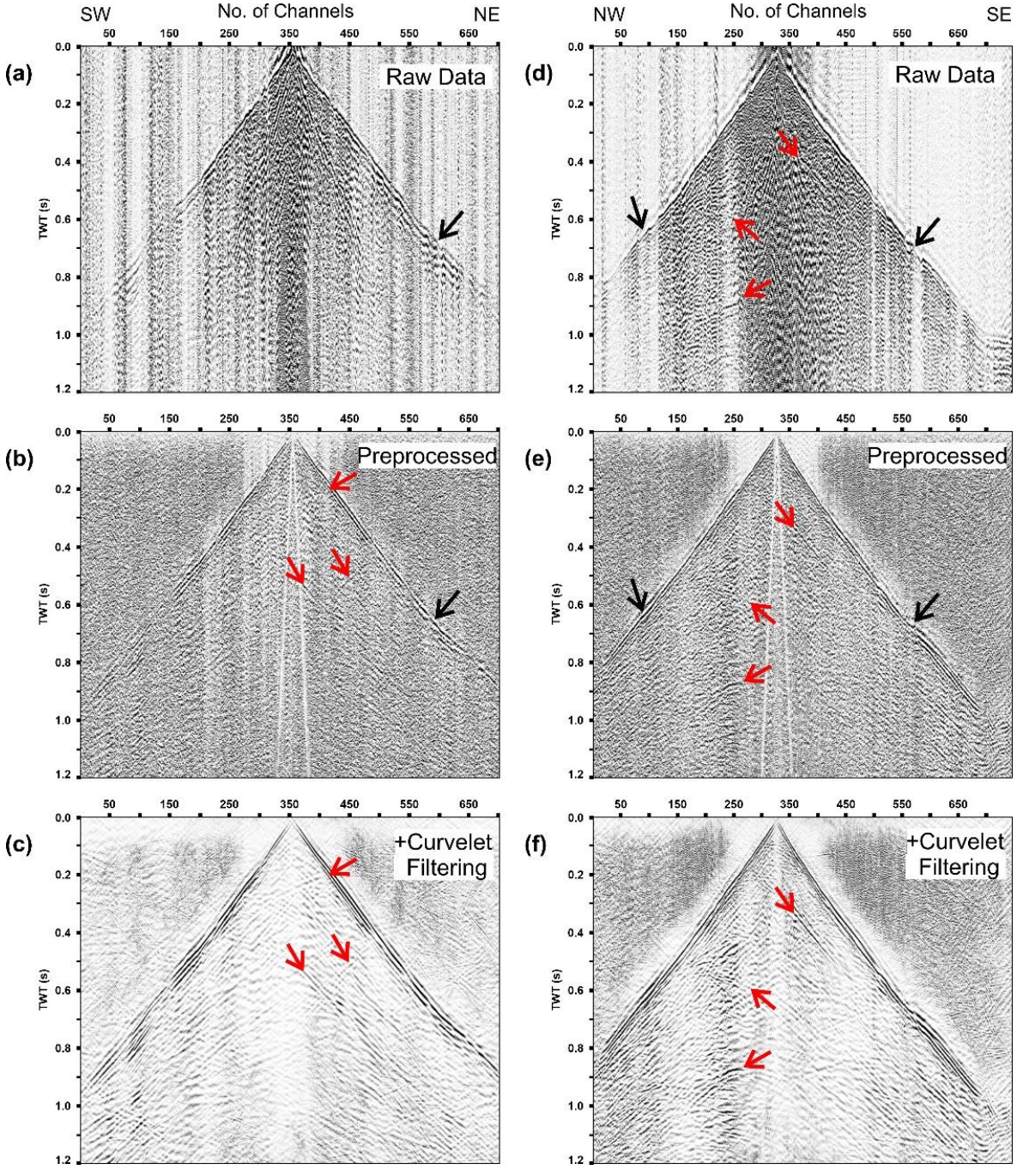

Figure 4: Result of data preprocessing applied to profiles L1000 and L2000 (a) Raw shot gather for profile L1000, (b) data with full preprocessing without the top-mute, and (c) is same as (b) with curvelet filtering. Trace balancing was applied for presentation purposes. (d), (e) and (f) are the same as (a), (b) and (c) for profile L2000. Black arrows show the correction of first arrivals due to the heterogenous near-surface weathered layer. Red arrows mark the comparative enhancement/preservation of reflectivity in the raw shot gathers.

https://doi.org/10.5194/egusphere-2025-496
Preprint. Discussion started: 6 March 2025

4.1 Depth-domain imaging

Along with PoSTM, we also tested Kirchhoff prestack depth migration (KPreSDM) due to its ability to better handle the complexity of the medium. To avoid the artifacts arising from a strict 2D migration of a crooked line, we performed KPreSDM in 3D mode (Singh and Malinowski, 2022, 2023). We used the migration code of Hloušek et al. (2015) working in the shot-domain. The computational domain for KPreSDM is shown as black boxes in Figure 1c. Depth migration parameters were kept similar for both profiles given the same acquisition setup and underlying geology in the area. For profiles L1000 and L2000, the grid dimensions are 701 x 141 x 434 and 735 x 168 x 434 (inline x crossline x depth) with a uniform grid spacing of 15 m. Similarly to PoSTM, a migration velocity of 6 km/s was used, however, KPreSDM was also tested for a scan of velocities in the range of ~5 – 6.5 km/s.

5. Results

Processing and time/depth imaging of the seismic data resulted in portraying several reflective packages at various depths of the subsurface. Figure 5 shows imaging results for profile L1000. Figure 5a shows the standard DMO-PoSTM sections. The origin (zero depth) is at 300 m a.s.l. and is the same for all the results presented in this article. Reflections down to a depth range of ~5 – 6 km are imaged. Events are less focussed in the first kilometre, although there are hints of steep reflectors projecting towards the surface (see black arrows labelled SF1-SF4). Other prominent reflections imaged at various depths are also marked by the black arrows. Arcuate reflectivity is mapped in the central area of the profile (marked by blue arrows). Its top is mapped at a depth of ~1.6 km with a clearly visible northeastern flank. A near-horizontal reflector at a depth of ~2.8 km (marked as FR) appears to crosscut the northeastern flank of the curved reflector around CDP ~875. A major reflector down-dipping from the southwestern end of the profile (starting at ~1 km depth) appears to be crosscutting the southwestern flank of the curved reflector (marked as DR1 and DR2). There is also the presence of several cross-cutting reflectors in the area (red arrows, CF1 and CF2). Higher reflectivity (~1 km) is mapped in the southwestern end of the profile in the depth range of ~1 – 3 km bounded by the reflector DR1. Reflectors mapped between CDPs 725 – 1200 (SF2, SF3, SF4) and depth up to ~2 – 3 km have an up-dip movement towards the surface. A dipping reflectivity is also mapped in the depth range of ~5 – 6 km (marked as LR1 and LR2). Compared to the KOSE2018 profile (Fig. 2), the new acquisition and processing produced abundant reflectivity in the area at various depths which was generally absent/poorly focussed, especially around the target area (compare Fig. 5a with Fig. 2).

Figure 5b shows the result for KPreSDM. The inline location is shown by the red line in Figure 1c. The inline crosscuts the curved CDP line as a straight line, therefore the assessment is only done on a comparative basis. In overall, the events for KPreSDM results are much more focused and continuous compared to DMO-PoSTM results. For example, the continuity of up-dip events between CDPs 725 – 1200 (SF2, SF3, SF4) is much better imaged. The central curved reflectivity is also

https://doi.org/10.5194/egusphere-2025-496
Preprint. Discussion started: 6 March 2025

delineated better along with other events except the reflectors imaged at deeper depths marked as LR1 and LR2, for which higher migration velocities are required (compare Fig. 5a with 5b).

205

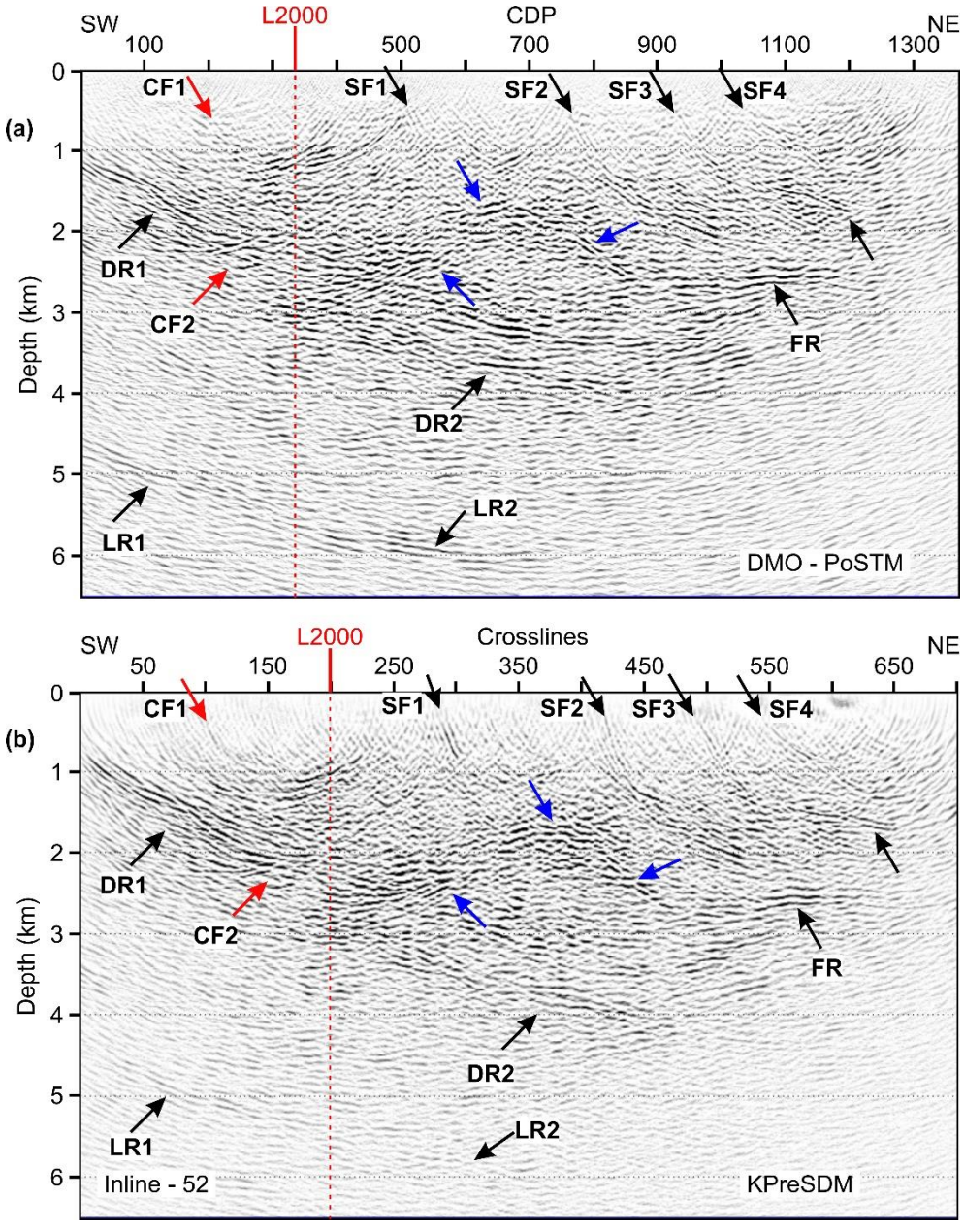

Figure 5: Imaging results for profile L1000. (a) 2D DMO-PoSTM (b) 3D KPreSDM (central inline). Black arrows show delineated reflectors at various depths and blue arrows mark the likely extent of the curved reflectivity. Red arrows mark the presence of crosscutting reflectors. The red dashed line shows the intersection location of profile L2000 with L1000.

https://doi.org/10.5194/egusphere-2025-496
Preprint. Discussion started: 6 March 2025

Figure 6 shows imaging results for profile L2000. Figure 6a shows the result for DMO-PoSTM. Black arrows mark different reflectors mapped in the area at various depth levels. Similarly to profile L1000, events are less focussed in the first kilometre with some visible reflectivity marked by black arrows (SF1 and SF2). There are hints of several cross-cutting events at the regional scale, although these events are too weak to mark their clear extents (red arrows, CF1 and CF2). The reflector marked as CF1 is delineated clearly up to a depth of ~4 km. Like in profile L1000, a horizontal reflector is also mapped at a depth of ~2.8 km (black arrows, FR). There is also the presence of deeper reflectivity marked by black arrows (LR1, depth ~4 km) and LR2 (depth ~5 km). A package of dipping reflectivity at the southeastern end of the profile is also mapped at a depth of ~1 – 2 km (marked as DR). Figure 6b shows results for KPreSDM. The inline location is shown as the red line in Fig. 1c. Same as for profile L1000, KPreSDM results are better focussed than DMO-PoSTM results (compare Fig. 6a with 6b). A notable difference can be seen for the reflector (CF3, red arrows) at CDP ~450 which is almost absent in the DMO-PoSTM result.

https://doi.org/10.5194/egusphere-2025-496
Preprint. Discussion started: 6 March 2025

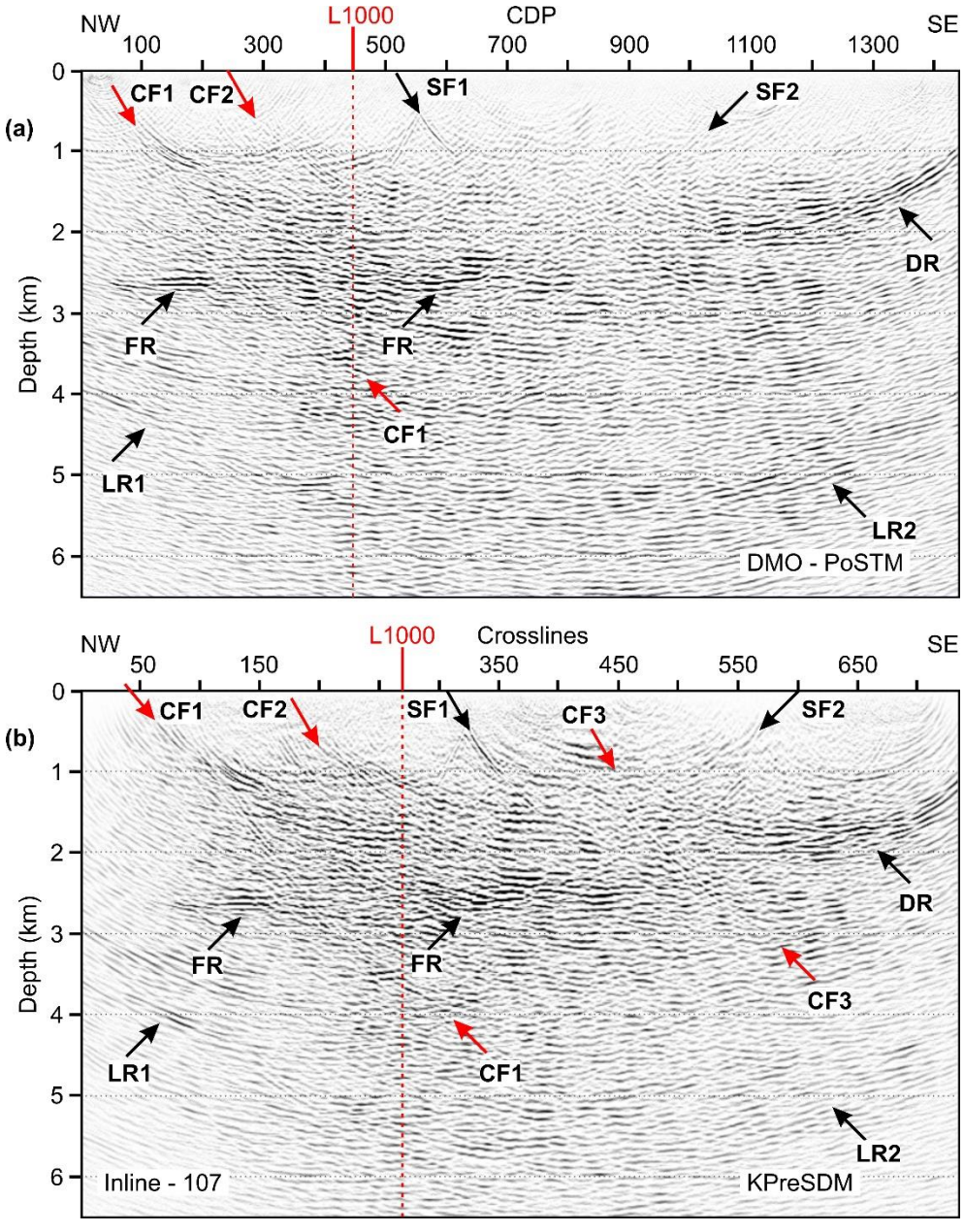

Figure 6: Imaging results for profile L2000. (a) 2D DMO-PoSTM, (b) 3D KPreSDM (central inline). Black arrows show imaged reflectivity at various depths in the area. Red arrows mark the steeply dipping cross-cutting reflectors. The red dashed line shows the intersection location of profile L1000 with L2000.

6. Interpretation and Discussion

The interpretation of the reflectivity mapped in the study area is challenging due to the presence of only one drillhole as a direct measurement. However, its origin can be associated with the presence of dykes, faults, and lithological contacts present

https://doi.org/10.5194/egusphere-2025-496
Preprint. Discussion started: 6 March 2025

in the area. The top of the magma conduit was successfully imaged with reflections mapped until the depth of ~5 – 6 km. The internal structure of the magma conduit seems more complex than its present understanding with hints of fault-like structures cross-cutting the intrusion. The obtained results were correlated with the initial (i.e. pre-seismic) geological model.

For the interpretation, KPreSDM results were preferred as they provided improved imaging with better continuity compared to DMO-PoSTM results (see the comparison in Fig. 5 and 6). Figure 7 shows the cross-sectional view of the KPreSDM results for both profiles. KPreSDM results are extracted along the same CDP processing line (green line, Fig. 1c) at which the DMO-PoSTM results are shown in Figures 5a and 6a. Figure 7a shows a view towards the west from the east direction. The drill hole is shown along profile L1000. It is to be noted that the processing line intersects the drillhole at a steep angle, so only a part of the drillhole is visible from this direction. An enlarged view of the cross-section of the drillhole is shown in the inset on the right. The up-dip reflector is marked by the red arrow in the inset upon projection crosscuts at ~600 m depth section of the drillhole. This reflector possibly represents the cross-cutting diabase encountered during the drilling (see Fig. 1, 3). The end of the drillhole where mafic-ultramafic rocks were encountered matches well with the top of the arcuate reflectivity. From this, it can be inferred that the curved reflectivity is representative of the mafic intrusion present in the area. Figure 7b again shows KPreSDM results from a view towards the northeast. Higher reflectivity is observed in the western part of the survey with the presence of several steep reflectors dipping towards the east and south direction (see red arrows, compare with CF1 & CF2 in Fig. 5a and CF1 in Fig. 6a, respectively). This possibly shows the presence of multiple larger fault systems present at a regional level in the area. Higher reflectivity only on the southwest side of the fault ‘CF1’ suggests it to be an overthrust fault which upon projection coincides with the banded iron formation occurrence that runs parallel to the mafic intrusion (marked by the red arrow in Fig. 1c). A large package of dipping reflectors is mapped on the southeastern end (marked by the blue arrow). There are no direct measurements available in this part of the area, but this higher package of reflectivity could be associated with the Korpua Iron Ore Intrusion (Makkonen, 1972) (see Fig. 1c for location). Interpretation of all the events observed in the seismic image is not possible at this stage.

Figure 8 shows a cross-sectional view of KPreSDM results against the initial geological model. The model includes a magma conduit, which was built based on the density model obtained from gravity inversion with constraints from the drillhole data. Figure 8a shows the view towards the west direction (same as in Fig. 7a). The modelled mafic intrusion correlates well with the mapped reflectivity. It is well-bounded within the mapped reflectivity in the central area as well as some prominent internal reflectivity (red arrows) which means that the internal geological structure of the mafic intrusion bears more complexity than what was thought of as a single lithological unit. Figure 8b is the same as Figure 8a with the projected outline of the magma conduit (dashed contour). Black dotted lines show different mapped reflectors in the area. There are impressions of major faults/lithological units cross-cutting the intrusion otherwise too weak to be marked distinctively. It can be inferred that there might be a second magma conduit between the exposed Koillismaa intrusion and Näränkävaara intrusion of the KLIC. The up-dip direction of the mapped faults above the magma conduit reached by the drilling faces opposite directions towards the

https://doi.org/10.5194/egusphere-2025-496
Preprint. Discussion started: 6 March 2025

northeast and southwest directions. These may be attributed to different lithological units resulting from the uplifting of the known magma conduit, or, they represent diabase veins mapped on the surface area.

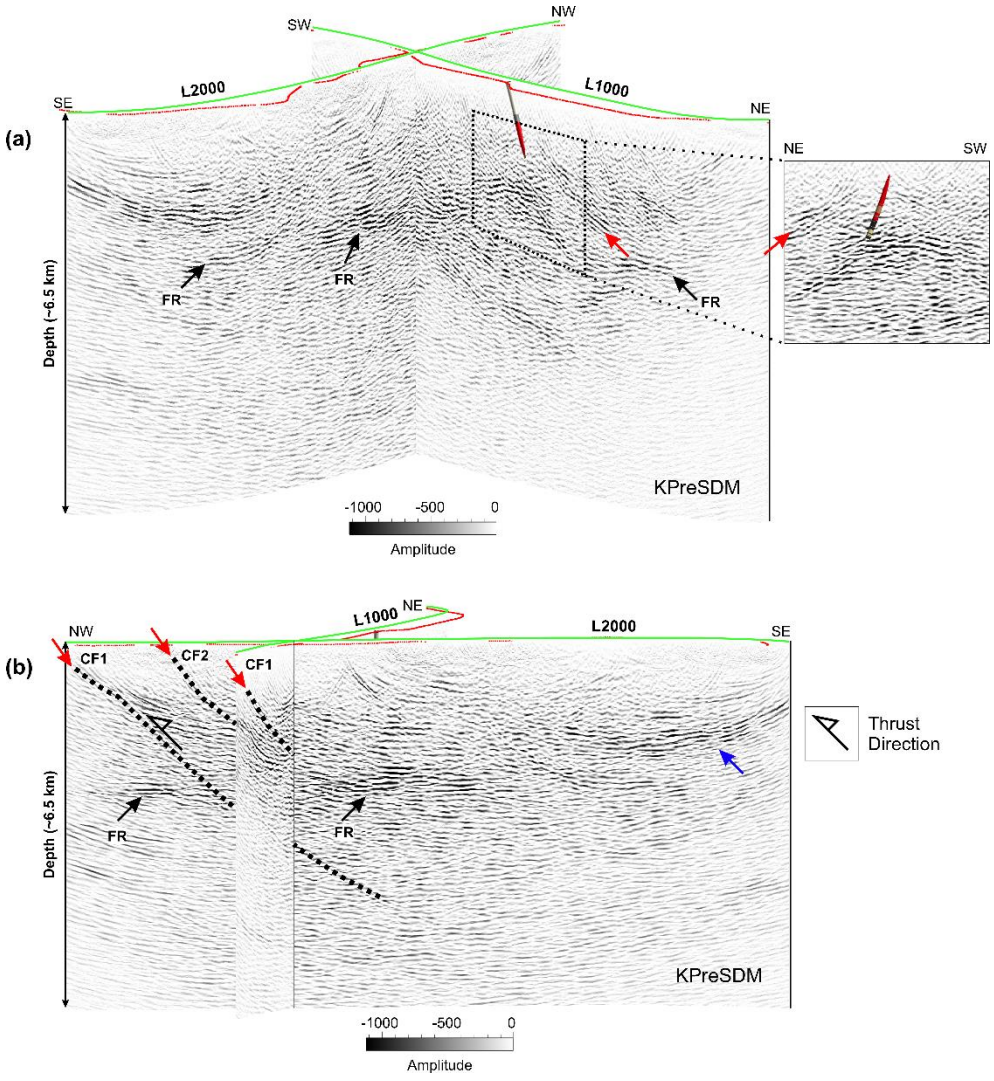

265 **Figure 7: Cross-sectional view of (a) KPreSDM result (b) same as (a) from a different view angle perspective. Insets in (a) show an enlarged section of (a) around the borehole location. Red, blue, and black arrows highlight reflectors used for the interpretation. The green line is the CDP line shown in Figure 1c and the red dots show source locations along the profiles. Dotted lines represent mapped faults in the area.**

https://doi.org/10.5194/egusphere-2025-496
Preprint. Discussion started: 6 March 2025

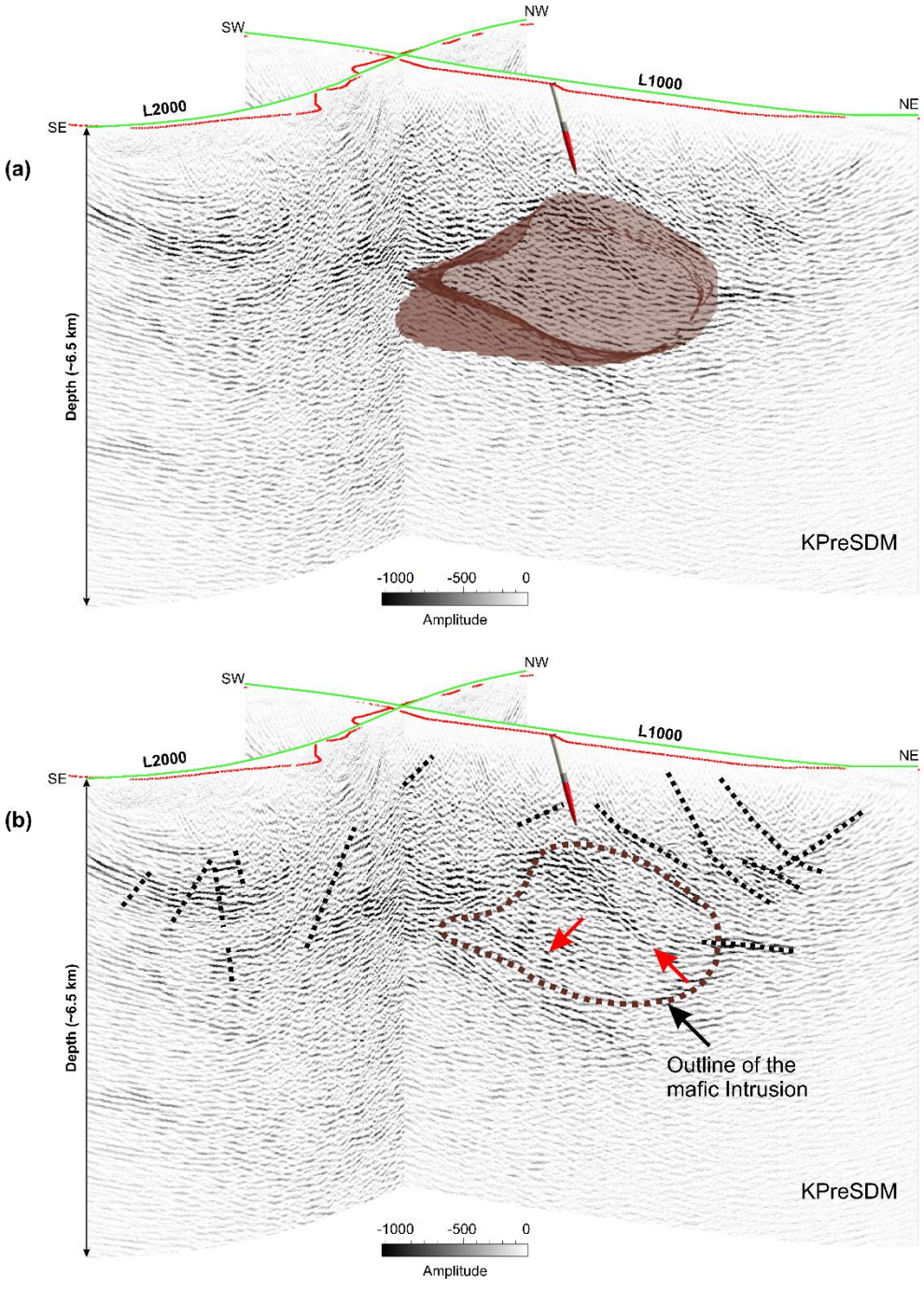

Figure 8: (a) Cross-sectional view of KPreSDM with the initial geological model of the mafic intrusion (dashed contour) (b) same as (a) with the highlighted outline of the intrusion (dashed closed contour). Black dashed lines show the main events. The green line shows the CDP line shown in Figure 3c, and the red dots show the source location along the profiles.

https://doi.org/10.5194/egusphere-2025-496
Preprint. Discussion started: 6 March 2025

7. Conclusions

Two seismic profiles were acquired within the SEEMS DEEP project to map the regional reflectivity and constrain the geometrical architecture of the deep-seated Koillismaa magma conduit. Depth-domain imaging (KPreSDM) provided more focused images with better continuity than DMO-PoSTM imaging. Several reflections are mapped at various depths whose origin can be associated with the presence of dykes, faults, and lithological contacts in the area. Regional faults were also imaged with reflectivity down to a depth of ~5 – 6 km. The top of the magma conduit associated with KLIC is successfully revealed which was one of the main aims of the SEEMS DEEP project. The internal structure of the magma conduit seems more complex than its present understanding with hints of fault-like structures cross-cutting the intrusion. It is interpreted that there might be a second magma conduit between the exposed Koillismaa intrusion and Näränkävaara intrusion of the KLIC. The two profiles' cross-cutting proximity proved advantageous in constraining the mapped regional-scale reflectivity in the area, leading to a more detailed understanding of the structural geology associated with the intrusion. This will tremendously help build a more detailed geological model of the Koillismaa area.

Data availability

Data associated with this research are available per request to the project coordinator: Uula Autio (uula.autio@gtk.fi), Geological Survey of Finland, Vuorimiehentie 5, 02151 Espoo, Finland.

Team list

Jochen Kamm, Cedric Patzer, Veera Pajunen, Toni Eerola, Tuija Luhta, Viveka Laakso (Geological Survey of Finland (GTK), Finland); Mathieu Darnet, Francois Bretaudeau, Simon Vedrine, Bitnarae Kim, Florent Beaubois, Jacques Deparis (French Geological Survey (BRGM), France); Szymon Oryński (Institute of Geophysics, Polish Academy of Sciences Warsaw (IGF PAN), Poland); Thomas Kalscheuer, Karol Sierszen, Mehrdad Bastani (Uppsala University, Sweden); Catherine Truffert, Fabrice Vermeersch, Julien Gance (IRIS Instruments, France); Łukasz Sito (Geopartner Geofizyka, Poland); Antti Kivinen, Janne Kaukolinna (GRM-services Oy, Finland); Yuriy Koltun (Laakso Minerals Oy, Finland)

Author contribution

AG, MM, and SH obtained funding. BS, AG, and MM designed the 2D survey. BS, AG, MM, SH, and MW contributed to the data acquisition. BS performed the signal processing for the seismic dataset used for DMO-PoSTM and PreSDM. AG contributed to the implementation of curvelet denoising to the seismic dataset. BS and MM QC'ed the signal processing results at various stages. BS, AG, and MM interpreted the results. BS, MM, and TK contributed to the interpretation of the results.

https://doi.org/10.5194/egusphere-2025-496
Preprint. Discussion started: 6 March 2025

BS wrote the manuscript's main content with major contributions from AG & MM, and other authors. All authors contributed to the final interpretation and discussion of the results.

Competing interests

The contact author has declared that neither they nor their co-authors have competing interests. However, one of the authors (MM) is a member of the editorial board of Solid Earth.

Acknowledgments

We are greatly thankful to the entire SEEMS DEEP field crew for helping in the acquisition of the data. 3C seismic receivers were used from the FINNSIP seismic instrument pool (FLEX-EPOS, Research Council of Finland 328776) and electric field sensors from the Geophysical Instrument Pool Potsdam (GIPP) were used. Globe Claritas™ under the academic license from Petrosys Ltd. and Seismic Unix was used for the data processing and visualization. Thanks to Mira Geoscience for special licensing terms to use Geoscience Analyst software. We thank TU Freiberg, Germany for allowing us to use their in-house code for depth-domain imaging. Curvelet denoising algorithm was taken from the CURVELAB project (www.curvelet.org). We acknowledge Google for using the map of Finland (Map data ©2025 Google, GeoBasis-DE/BKG (©2009)).

Financial support

SEEMS DEEP is a part of the ERA-MIN3 Joint call 2021 (National funding agencies: Finland: Business Finland (640/31/2022), France: ANR (ANR-22-MIN3-0006-02), Sweden: VINNOVA (2022-00209), Poland: NCBR (ERA-MIN3/1/113/SEEMSDEEP/2022).

References

Alapieti, T.: The Koillismaa Layered Igneous Complex, Finland - Its Structure, Mineralogy and Geochemistry with Emphasis on the Distribution of Chromium, The Koillismaa Layered Igneous Complex, Finland - Its Structure, Mineralogy and Geochemistry with Emphasis on the Distribution of Chromium, 1982.

EU Critical Raw Materials Act: Regulation (EU) 2024/1252 of the European Parliament and of the Council of 11 April 2024 establishing a framework for ensuring a secure and sustainable supply of critical raw materials and amending Regulations (EU) No 168/2013, (EU) 2018/858, (EU) 2018/1724 and (EU) 2019/1020.: https://eur-lex.europa.eu/eli/reg/2024/1252/oj, last access: 12 November 2024.

Autio, U., Darnet, M., Górszczyk, A., Kamm, J., Heinonen, S., Malinowski, M., Kim, B., Singh, B., Vedrine, S., Bretaudeau, F., Patzer, C., Karinen, T., Kalscheuer, T., Truffert, C., Wojdyła, M., Kivinen, A., and Koltun, Y.: Integrating Seismic and Electromagnetic Methods for Deep Mineral Exploration – Results from the SEEMS DEEP Project, NSG 2024 5th Conference on Geophysics for Mineral Exploration and Mining, 1–5, https://doi.org/10.3997/2214-4609.202420147, 2024.

Barnes, S. J., Cruden, A. R., Arndt, N., and Saumur, B. M.: The mineral system approach applied to magmatic Ni–Cu–PGE sulphide deposits, Ore Geology Reviews, 76, 296–316, https://doi.org/10.1016/j.oregeorev.2015.06.012, 2016.

https://doi.org/10.5194/egusphere-2025-496
Preprint. Discussion started: 6 March 2025

Bellefleur, G., Schetselaar, E., White, D., Miah, K., and Dueck, P.: 3D seismic imaging of the Lalor volcanogenic massive sulphide deposit, Manitoba, Canada, Geophysical Prospecting, 63, 813–832, https://doi.org/10.1111/1365-2478.12236, 2015.

Bleeker, W. and Ernst, R.: Short-lived mantle generated magmatic events and their dyke swarms: The key unlocking Earth's paleogeographic record back to 2.6 Ga, Dyke Swarms—Time Markers of Crustal Evolution, 3–26, 2006.

Cheraghi, S., Naghizadeh, M., Snyder, D., Haugaard, R., and Gemmell, T.: High-resolution seismic imaging of crooked two-dimensional profiles in greenstone belts of the Canadian shield: results from the Swayze area, Ontario, Canada, Geophysical Prospecting, 68, 62–81, https://doi.org/10.1111/1365-2478.12854, 2020.

Ciborowski, T. J. R., Kerr, A. C., Ernst, R. E., McDonald, I., Minifie, M. J., Harlan, S. S., and Millar, I. L.: The Early Proterozoic Matachewan Large Igneous Province: Geochemistry, Petrogenesis, and Implications for Earth Evolution, Journal of Petrology, 56, 1459–1494, https://doi.org/10.1093/petrology/egv038, 2015.

European Commission Report: Directorate-General for Internal Market, Industry, Entrepreneurship and SMEs (European Commission), Grohol, M., and Veeh, C.: Study on the critical raw materials for the EU 2023: final report, Publications Office of the European Union, 2023.

Gislason, G., Heinonen, S., Salmirinne, H., Konnunaho, J., and Karinen, T.: KOSE-Koillismaa Seismic Exploration survey: Acquisition, processing and interpretation, GTK: n työraportti-GTK Open File Work Report, 2019.

Górszczyk, A., Malinowski, M., and Bellefleur, G.: Enhancing 3D post-stack seismic data acquired in hardrock environment using 2D curvelet transform, Geophysical Prospecting, 63, 903–918, https://doi.org/10.1111/1365-2478.12234, 2015.

Heaman, L. M.: Global mafic magmatism at 2.45 Ga: Remnants of an ancient large igneous province?, Geology, 25, 299–302, https://doi.org/10.1130/0091-7613(1997)025<0299:GMMAGR>2.3.CO;2, 1997.

Heinonen, S., Nousiainen, M., Karinen, T., and Häkkinen, T.: Are Seismic P-Wave Velocities Capable of Revealing The Deep-Seated Prospective Intrusion?, NSG2022 4th Conference on Geophysics for Mineral Exploration and Mining, 1–5, https://doi.org/10.3997/2214-4609.202220167, 2022.

Hloušek, F., Hellwig, O., and Buske, S.: Improved structural characterization of the Earth's crust at the German Continental Deep Drilling Site using advanced seismic imaging techniques, Journal of Geophysical Research: Solid Earth, 120, 6943–6959, https://doi.org/10.1002/2015JB012330, 2015.

Karinen, T.: The Koillismaa intrusion, northeastern Finland: evidence for PGE reef forming processes in the layered series, Geological Survey of Finland, 2010.

Karinen, T., Heinonen, S., Konnunaho, J., Salmirinne, H., Lahti, I., and Salo, A.: Koillismaa Deep Hole–Solving the mystery of a geophysical anomaly, in: Lithosphere 2021, eleventh symposium on structure, composition and evolution of the lithosphere, Programme and Extended Abstracts, 55–58, 2021a.

Karinen, T., Salmirinne, H., Lahti, I., Konnunaho, J., S., H., and Salo, A.: The Koillismaa Deep Hole: insight to anomalous mafic intrusion, 38–41, https://doi.org/10.31241/ARLIN.2021.009, 2021b.

Köykkä, J., Lahtinen, R., and Manninen, T.: Tectonic evolution, volcanic features and geochemistry of the Paleoproterozoic Salla belt, northern Fennoscandia: From 2.52 to 2.40 Ga LIP stages to ca. 1.92–1.90 Ga collision, Precambrian Research, 371, 106597, https://doi.org/10.1016/j.precamres.2022.106597, 2022.

Makkonen, V.: Korpuan Jatkotutkimus. Rautaruukki Oy Research Report Ou 16/72, 1972.

https://doi.org/10.5194/egusphere-2025-496
Preprint. Discussion started: 6 March 2025

Malehmir, A., Durrheim, R., Bellefleur, G., Urosevic, M., Juhlin, C., White, D. J., Milkereit, B., and Campbell, G.: Seismic methods in mineral exploration and mine planning: A general overview of past and present case histories and a look into the future, GEOPHYSICS, 77, WC173–WC190, https://doi.org/10.1190/geo2012-0028.1, 2012.

Malehmir, A., Maries, G., Bäckström, E., Schön, M., and Marsden, P.: Developing cost-effective seismic mineral exploration methods using a landstreamer and a drophammer, Sci Rep, 7, 10325, https://doi.org/10.1038/s41598-017-10451-6, 2017.

Malinowski, M., Brodic, B., Martinkauppi, I., Koskela, E., and Laakso, V.: Distributed acoustic sensing vertical seismic profiling in hardrock environment: case study from Koillismaa drillhole, Finland, 84th EAGE Annual Conference & Exhibition, 1–5, https://doi.org/10.3997/2214-4609.2023101043, 2023.

Malinowski, M., Heinonen, S., Górszczyk, A., Singh, B., Sito, L., Karinen, T., and Autio, U.: A Novel 3D Seismic Survey over the 2.5-2.4 Ga Koillismaa Layered Intrusion Complex, Finland, NSG 2024 5th Conference on Geophysics for Mineral Exploration and Mining, 1–5, https://doi.org/10.3997/2214-4609.202420077, 2024.

Markovic, M., Maries, G., Malehmir, A., Ketelhodt, J. von, Bäckström, E., Schön, M., and Marsden, P.: Deep reflection seismic imaging of iron-oxide deposits in the Ludvika mining area of central Sweden, Geophysical Prospecting, 68, 7–23, https://doi.org/10.1111/1365-2478.12855, 2020.

Milkereit, B., Berrer, E. K., King, A. R., Watts, A. H., Roberts, B., Erick, A., Eaton, D. W., Wu, J., and Salisbury, M. H.: Development of 3-D seismic exploration technology for deep nickel-copper deposits—A case history from the Sudbury basin, Canada3-D Seismic Exploration Technology, Geophysics, 65, 1890–1899, https://doi.org/10.1190/1.1444873, 2000.

Nedimović, M. R. and West, G. F.: Crooked-line 2D seismic reflection imaging in crystalline terrains: Part 2, migration, GEOPHYSICS, 68, 286–296, https://doi.org/10.1190/1.1543214, 2003.

Nousiainen, M., Heinonen, S., and Karinen, T.: Petrophysics of the Koillismaa drill hole, in: TWELFTH SYMPOSIUM ON THE STRUCTURE, COMPOSITION AND EVOLUTION OF THE LITHOSPHERE, 131, 2022.

Ripley, E. M. and Li, C.: Chapter 3 - Metallic Ore Deposits Associated With Mafic to Ultramafic Igneous Rocks, in: Processes and Ore Deposits of Ultramafic-Mafic Magmas through Space and Time, edited by: Mondal, S. K. and Griffin, W. L., Elsevier, 79–111, https://doi.org/10.1016/B978-0-12-811159-8.00004-4, 2018.

Salmirinne, H. and Iljina, M.: Koillismaan kerrosintruusiokompleksin tulokanavamuodostuman painovoimatulkinta ja alueen malmimahdollisuudet (osa 1), Geologian Tutkimuskeskus Q, 21, 1, 2003.

Schulz, K. J., Woodruff, L. G., Nicholson, S. W., Ii, R. R. S., Piatak, N. M., Chandler, V. W., and Mars, J. L.: Occurrence model for magmatic sulfide-rich nickel-copper-(platinum-group element) deposits related to mafic and ultramafic dike-sill complexes, Scientific Investigations Report, U.S. Geological Survey, https://doi.org/10.3133/sir20105070I, 2014.

Singh, B. and Malinowski, M.: Depth Imaging of Crooked Seismic Profiles in Hardrock Environment: Is 2D Enough?, NSG2022 4th Conference on Geophysics for Mineral Exploration and Mining, 1–5, https://doi.org/10.3997/2214-4609.202220169, 2022.

Singh, B. and Malinowski, M.: Seismic Imaging of Mineral Exploration Targets: Evaluation of Ray-vs. Wave-Equation-Based Pre-Stack Depth Migrations for Crooked 2D Profiles, Minerals, 13, 264, 2023.

Singh, B., Górszczyk, A., Malinowski, M., Heinonen, S., Autio, U., Wojdyła, M., and Kamm, J.: Mapping Regional Reflectivity of Mineral-prone Koillismaa Layered Intrusion Complex in Northern Finland using Crooked Seismic Profiles,

https://doi.org/10.5194/egusphere-2025-496
Preprint. Discussion started: 6 March 2025

NSG 2024 5th Conference on Geophysics for Mineral Exploration and Mining, 1–5, https://doi.org/10.3997/2214-4609.202420162, 2024.

Skyttä, P., Piippo, S., Kloppenburg, A., and Corti, G.: 2. 45 Ga break-up of the Archaean continent in Northern Fennoscandia: Rifting dynamics and the role of inherited structures within the Archaean basement, Precambrian Research, 324, 303–323, https://doi.org/10.1016/j.precamres.2019.02.004, 2019.

Tirronniemi, J., Bischoff, A., Malinowski, M., Autio, U., Karinen, T., Lukkarinen, V., Heinonen, S., Mikkola, P., Leskelä, T., and Patzer, C.: Koillismaa Deep Hole–Final Report, GTK Open File Work Report, 73-pp, 2024.